Constitutive activation of cellular immunity underlies the evolution of resistance to infection

Alexandre B. Leitão*, Ramesh Arunkumar*, Jonathan P. Day, Emma M. Geldman, Francis M. Jiggins

Department of Genetics, University of Cambridge, Cambridge, United Kingdom

* contributed equally

Abstract

Organisms rely on inducible and constitutive immune defences to combat infection. Constitutive immunity enables a rapid response to infection but may carry a cost for uninfected individuals, leading to the prediction that it will be favoured when infection rates are high. When we exposed populations of *Drosophila melanogaster* to intense parasitism by the parasitoid wasp *Leptopilina boulardi,* they evolved resistance by developing a more reactive cellular immune response. Using single-cell RNA sequencing, we found that immune-inducible genes had become constitutively upregulated. This was the result of resistant larvae differentiating precursors of specialized immune cells called lamellocytes that were previously only produced after infection. Therefore, populations evolved resistance by genetically hard-wiring an induced immune response to become constitutive.

Main

A fundamental division within immune systems is between induced and constitutive immune defences. Constitutive immunity is always active, even in the absence of infection. For example, uninfected individuals produce natural antibodies[1], immune cells and antimicrobial peptides (AMPs) [2]. In contrast, induced immune responses are triggered after infection, which frequently involve amplifying existing constitutive factors. This can include immune cells proliferating and differentiating, and the massive upregulation of AMPs and cyotoxic molecules [2]. Constitutive immunity is fast, allowing hosts to avoid becoming infected altogether or to rapidly clear infections. However, immune defences can be costly, diverting limited resources from other fitness-related traits [3] or damaging the host through immunopathology [4]. While induced immune responses only incur these costs after infection, they are always present for constitutive immunity, even in the absence of infection. This trade-off between speed and cost is predicted to govern the allocation of host investment into constitutive and induced immunity [5,6]. Theoretical models predict that the key parameter determining which type of defence should be favoured is the frequency that hosts are exposed to infection—more frequent exposure favours constitutive defences [5]. In support of this, bacteria tend to evolve phage resistance by altering surface receptors when exposure is high and rely on induced CRISPR-Cas immunity when exposure is low [7]. However, to our knowledge the key prediction that high rates of parasitism lead to induced immune responses becoming constitutively expressed has not been demonstrated.

39

40 To investigate these questions, we examined how the constitutive and induced
41 cellular immune defences of *Drosophila melanogaster* evolve under high parasite
42 pressure. Cellular immunity in *D. melanogaster* involves blood cells called
43 hemocytes, which play the equivalent role to leukocytes in vertebrates. In
44 uninfected larvae there are two morphological classes of hemocytes.
45 Plasmatocytes constitute the majority of cells and have diverse functions
46 including phagocytosis and AMP production [8]. Crystal cells are a less abundant
47 specialized cell type that produces the prophenoloxidase molecules PPO1 and
48 PPO2, which are processed into enzymes required for the melanization of
49 parasites [9]. Infection can trigger an induced response, where these cell types
50 proliferate, and cells called lamellocytes differentiate from plasmatocytes and
51 prohemocytes in the lymph gland [8]. Lamellocytes are large flat cells with a
52 specialised role in killing large parasites like parasitic wasps (parasitoids). When
53 a parasitoid injects its egg into *D. melanogaster* larvae, plasmatocytes adhere to
54 the egg. Then, as lamellocytes differentiate they create additional cellular layers
55 known as a 'capsule'. Finally, the capsule is melanised by the activity of
56 phenoloxidases produced in crystal cells and lamellocytes [9]. The melanin
57 physically encases the parasitoid and toxic by-products of the melanisation
58 reaction likely contribute to parasite killing [10].
59

60 There is substantial genetic variation in susceptibility to parasitoid infection
61 within *D. melanogaster* populations [11], and this is associated with differences in
62 hemocyte composition [12,13]. Here, we used a combination of experimental
63 evolution with physiological assays and single-cell RNA sequencing to examine

how a high rate of parasitism by the parasitoid wasp *L. boulardi* affects constitutive and induced immune defences.

The evolution of resistance is associated with a more reactive immune response

To investigate the evolution of the cellular immune response, we allowed genetically diverse populations of *D. melanogaster* to evolve under intense levels of parasitism. We established an outbred population from 377 wild-caught *D. melanogaster* females, and used this to found six experimental populations that were maintained at population sizes of 200 flies. In three of these populations, larvae were infected every generation, and flies that survived by encapsulating and melanising the wasp were used to establish the next generation (High Parasitism populations). The other three populations were maintained in the same conditions but without infection (No Parasitism populations). In line with previous studies [12,14], the High Parasitism populations increased in resistance over the generations (Fig. 1A, Selection regime x Generation: $\chi^2 = 91.41$, d.f.= 1, $p<10^{-15}$). After 33 generations, a mean of 76% of flies survived infection in the High Parasitism populations, compared to 10% in the No Parasitism controls.

As populations evolved resistance, they melanised parasitoids at a higher rate (Fig. 1A). This could result from increased basal reactivity of the encapsulation immune response, or because the flies are evolving to escape the effects of immunosuppressive molecules produced by the parasite. To distinguish these possibilities, we measured the ability of each population to react to an inert object. When a small volume of paraffin oil is injected into the larval haemocoel,

89 it remains as a sphere and can be encapsulated [15]. Populations that evolved
90 without parasitism show a very limited reaction to the oil droplets (Fig. 1B). In
91 contrast, approximately half of larvae from selected populations encapsulate the
92 oil droplet (Fig. 1B; Selection Regime: $F_{1,4}$=24.53, p=0.008). Therefore, high levels
93 of parasitism led to the cellular immune system evolving a more reactive
94 encapsulation response.

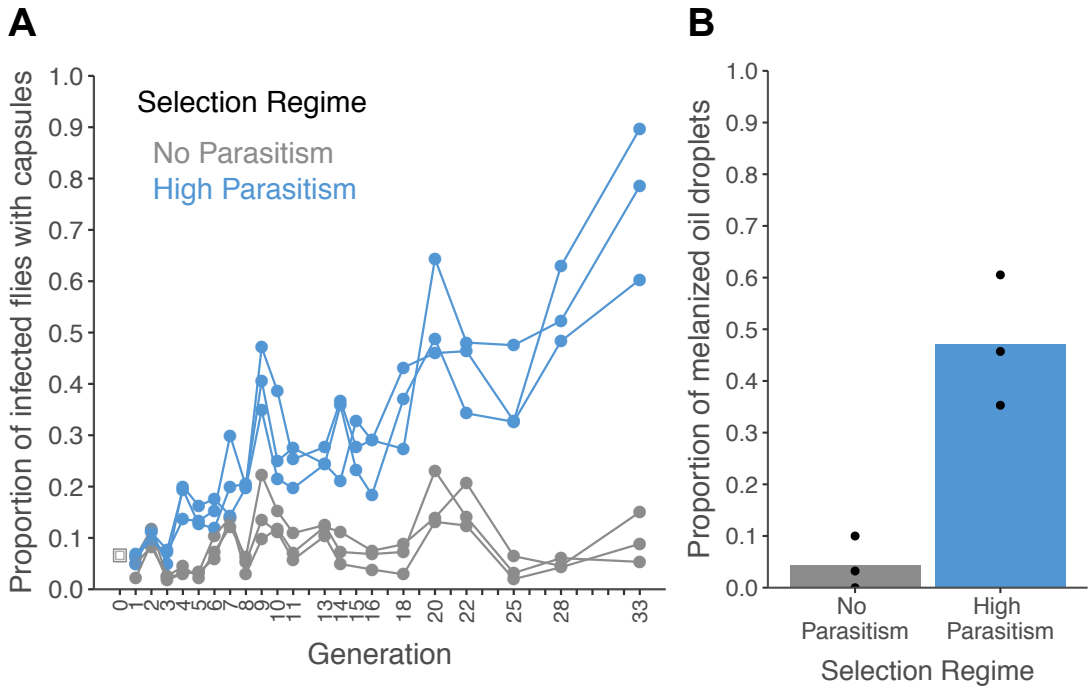

95

96 **Figure 1 Encapsulation rate during selection for parasitoid resistance.** (A) The
97 proportion of infected larvae that gave rise to adult flies with visible capsules. An
98 outbred population of *D. melanogaster* (source, grey square) was used to found six
99 populations that were parasitized every generation with *L. boulardi* (blue) or maintained
100 without infection (grey). (B) The proportion of larvae encapsulating oil droplets at
101 generation 33. Dots represent the proportion of larvae in replicate populations and bars
102 represent the mean per selection regime.

103

104

105

106 **Constitutive upregulation of immune-induced genes**

107 Underlying induced immune responses is a transcriptional response to infection,
108 so we examined how the hemocyte transcriptome altered in populations that
109 evolved under high levels of parasitism. We harvested hemocytes from
110 *Drosophila* larvae and sequenced the transcriptomes of individual cells using the
111 10X Genomics platform. Initially, we pooled the data from scRNA-seq to
112 investigate global changes in hemocyte gene expression. As expected, 48 hours
113 post infection there was a strong transcriptional response to infection (Fig. 2A, X
114 axis; Data S1). Strikingly similar transcriptional changes occurred in uninfected
115 flies that had evolved under high rates of parasitism for 26 generations (Fig. 2A,
116 Y axis; Data S1). Taking the 173 genes that had at least a 50% change in
117 transcript levels after infection or selection, in every case the direction of change
118 was the same after infection and adaptation to high parasitism (Fig. 2A; Data S1).
119 We verified that the evolved response mimicked the induced response by using
120 quantitative PCR (qPCR) to measure the expression of the lamellocyte marker
121 *atilla* and the anti-parasitoid effector gene *PPO3* (Fig. S1). Again, we found that
122 high rates of parasitism led to these immune-induced genes becoming
123 constitutively upregulated. Therefore, as populations evolved resistance, the
124 induced transcriptional response to infection has become genetically hard-wired
125 and constitutive.

126

127 We took the same approach to examine how the induced transcriptional
128 response to infection changed as populations evolved resistance. We found that
129 the transcriptional response to infection involved the same genes in the different

130 populations (Fig. 2B). However, the magnitude of the changes in gene expression
131 was substantially less in populations that had evolved under high parasite
132 pressure (Fig. 2B). Therefore, the increase in constitutive gene expression has
133 been matched by a decrease in induced expression. Again, this was verified by
134 qPCR (Fig. S1). Combining the constitutive and induced changes in gene
135 expression, the hemocyte transcriptome after infection is similar in the
136 populations that evolved under high levels of parasitism and the controls (Fig.
137 2C). Therefore, an induced response has become genetically fixed, as opposed to
138 selection leading to a greater total response.

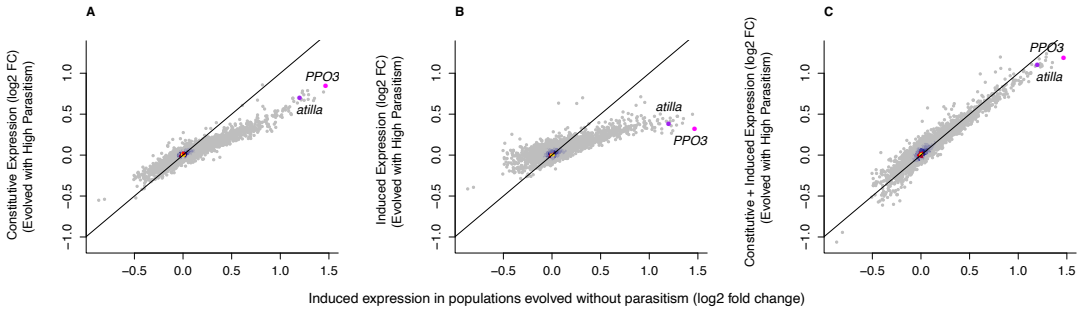

139 **Figure 2. Changes in gene expression following selection for resistance and**
140 **parasitoid infection.** (A) Constitutive gene expression following 26 generations of
141 selection for resistance to the parasitoid wasp *L. boulardi* (y-axis). (B) The induced
142 change in gene expression following infection with *L. boulardi* in populations selected for
143 resistance (y-axis). (C) The combined induced and constitutive change in gene
144 expression following selection for resistance and infection (y-axis). All are compared to
145 the change in gene expression following infection in populations maintained without
146 parasitoid infection (x-axis). The black diagonal indicates the 1:1 line. The genes *atilla*
147 and *PPO3* are highlighted. Colour represents the density of overlain points. Relative
148 expression is expressed as $\log_2$(fold change).

149

150 **scRNA-seq reveals novel hemocyte types**

151 The global changes in hemocyte transcriptomes could result from a change in the
152 relative proportion of cell types in the hemocyte population, or from a shift in
153 gene expression within existing cell types. The three classical *Drosophila*
154 hemocyte types were originally defined morphologically, but emerging single
155 cell transcriptomic data suggests that *Drosophila* hemocyte populations are more
156 complex than this [16–19]. Excluding cells that did not express the pan-hemocyte
157 markers *Hemese* or *Serpent* [20,21], we grouped 19,344 larval hemocytes into nine
158 clusters based on their transcriptomes (Fig. 3A). Neither infection nor selection
159 leads to the appearance of new cell states (Fig. 3B).

160 We identified two large clusters of plasmatocytes. The largest was PLASM1,
161 which we classify as the cycling plasmatocyte state as it had the greatest number
162 of replicating cells in the G2M or S phase (Fig. S2). The 5,712 cells in this cluster
163 had high expression of genes associated with plasmatocytes (*Col4a1*, *Pxn*, *eater*,
164 *Hml*, *NimC1*[21]) and actively replicating cells (*stg* [22], *polo*[23]and *scra*[24]) (Fig. S3).
165 The next largest cluster, PLASM2, contained 2,874 plasmatocytes that were
166 enriched for the genes encoding rRNA (Fig. S4) or involved in the ribosome
167 biogenesis (Data S3). There were two smaller plasmatocyte clusters. The AMP
168 cluster contained 196 cells with elevated expression of genes encoding
169 antimicrobial and antifungal peptides, including *Drs*, *Mtk* and *CecA1* (Lemaitre
170 and Hoffmann 2007, Fig. S4; Data S3). The MET cluster contained 283 cells with
171 high expression of the heat shock proteins *Hsp24* and *Hsp27* and genes involved
172 in organic acid metabolism (Fig. S4; Data S3). The crystal cells formed a single
173 cluster of 906 cells (Fig. S6). Three clusters of cells, LAM 1, 2 and 3, had elevated
174 expression of one or more lamellocyte marker genes [21] (Fig. S5) and contained
175 1,260, 5,104 and 3,000 cells respectively.

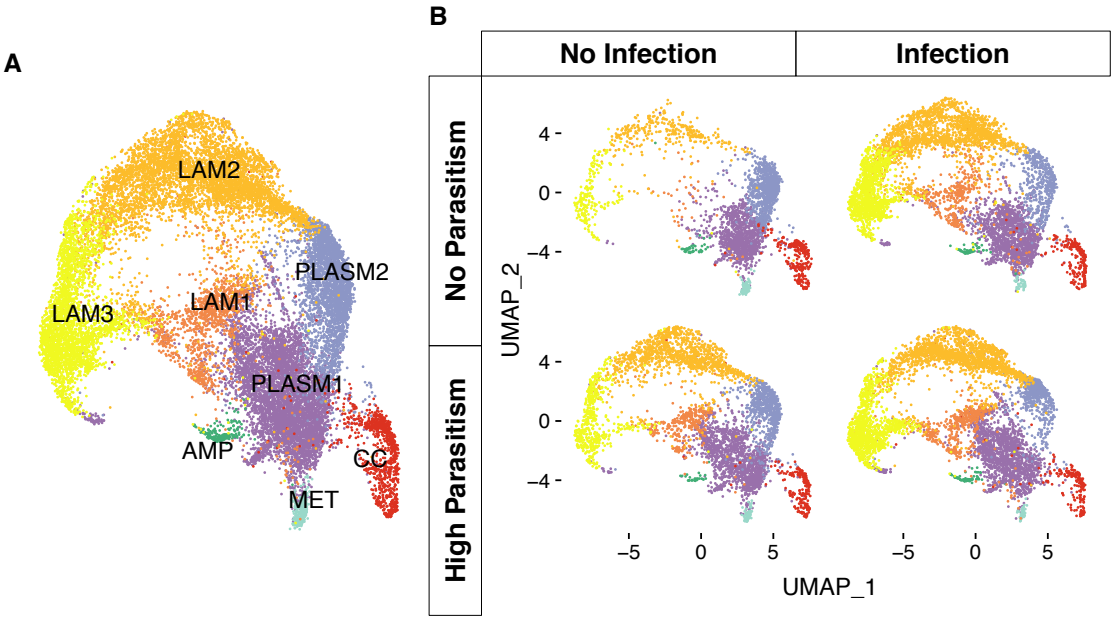

176 **Figure 3. Cell states of *Drosophila melanogaster* larval hemocytes.** Two-dimensional
177 UMAP projections and cell state classification. (A) All 19,344 cells combined. PLASM:
178 plasmatocytes; MET: metabolic plasmatocyte cluster; AMP: antimicrobial peptide
179 plasmatocyte cluster; LAM: lamellocytes; CC: crystal cells. (B) Cells from populations that
180 had undergone 26 generations of selection with no parasitism (top panels) or high
181 parasitism (bottom panels), and were either uninfected (left panels) or 48 hours post
182 infection (right panels). 64-333 million reads were sequenced in each of the eight 10X
183 libraries that we generated (Data S2). The number of cells detected per library ranged
184 from 787 to 3,463 (Fig. S6).

185

186 **Inducible cell states are present constitutively in resistant populations**

187 Lamellocytes are key effector cells in the anti-parasitoid immune response. In
188 populations that evolved without exposure to parasitoids, infection resulted in a
189 large increase in the number of cells in all three lamellocyte clusters (LAM1-3,
190 Fig. 3B and 4A). In populations that evolved under high levels of parasitism, this
191 inducible response become constitutive, with uninfected larvae having 3-5 fold
192 more cells in LAM1 and 2 (Fig. 4A). However, this was matched by a reduction in

193 the induced response, so the final number of cells in these clusters after infection
194 was similar regardless of whether the populations had adapted to high or low
195 parasitism rates (Fig. 4A). These results held when replicate populations were
196 analyzed separately (Fig. S7A, B) or when the number of cells in each library
197 were down-sampled to match the library with the least number of cells (Fig.
198 S7C). Therefore, high infection rates led to the inducible differentiation of
199 specialised immune cells becoming genetically fixed.

200 To investigate the developmental origins of this change, we reconstructed the
201 pathway by which plasmatocytes differentiate into mature lamellocytes. By
202 subclustering the cells and ordering them along a pseudotemporal scale, we
203 found a single lineage starting from the self-cycling plasmatocytes (PLASM1) and
204 ending in LAM3 (Figs. 4B). Along this lineage there was a decrease in cell
205 replication, with the largest fraction of cells in the G2M and S phase in PLASM1
206 and the largest fraction in G1 in LAM3 (Fig. S8). Importantly, controlling for the
207 effects of cell cycle had a negligible impact on the clustering (Table S1) and the
208 trajectory of lamellocyte differentiation (Fig. S9). The expression of the effector
209 gene *PPO3,* the lamellocyte marker *atilla* and other marker genes all increased as
210 cells progressed along this trajectory (Fig. 4C, 4D and S10, Data S4). On the other
211 hand, genes involved in extracellular matrix organization—a house-keeping
212 function of plasmatocytes [25,26]—were down-regulated as cells differentiated
213 (Data S5). Together, these results suggest that LAM1 cells are immature
214 lamellocytes, while LAM3 cells are mature lamellocytes. Comparing our
215 populations, the inducible production of LAM1 cells has become entirely
216 constitutive in the populations evolved under high rates of parasitism, while
217 much of the LAM3 response remains inducible. This suggests that high infection

218 rates result in the cellular immune response becoming 'primed' by constitutively

219 producing the precursors of the cells required for parasite killing.

220

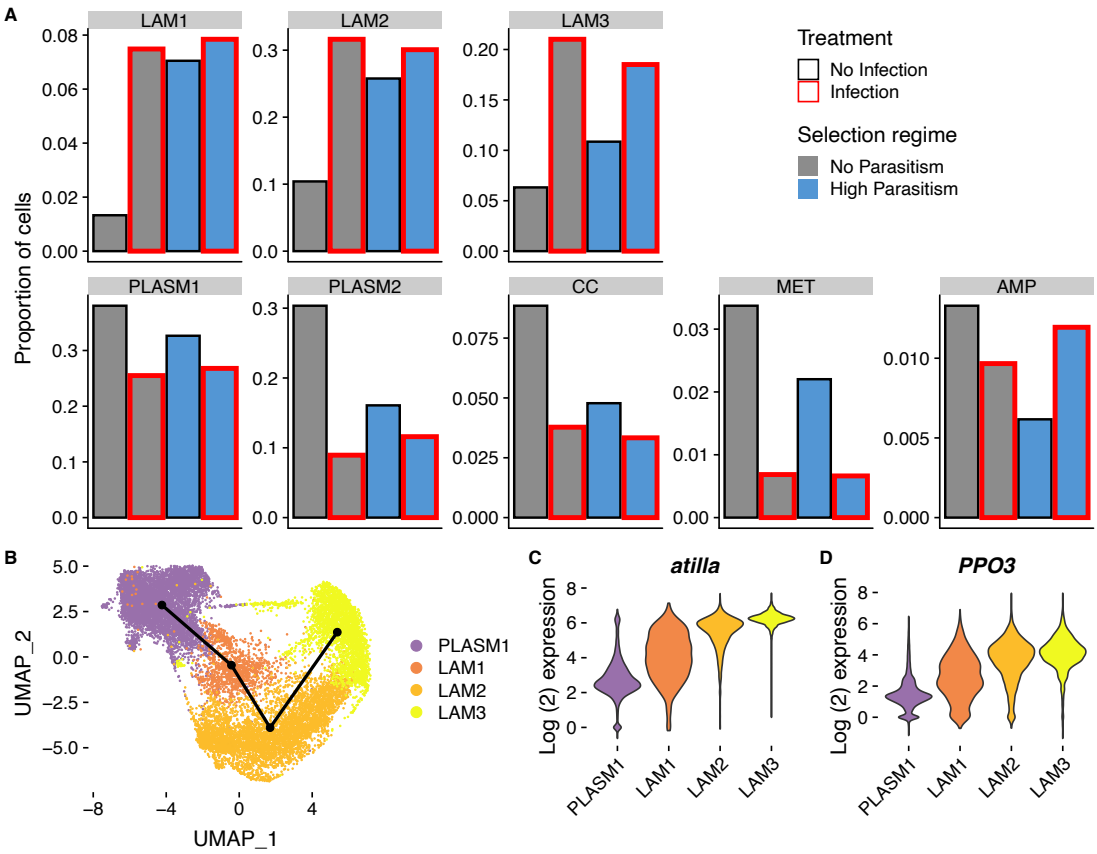

221

222 **Figure 4. Changes in cell state following infection and adaptation to high rates of**

223 **parasitism.** (A) Proportion of different cell states after infection and selection. (B)

224 Trajectory of lamellocyte differentiation. Plasmatocyte progenitors and lamellocytes

225 were subclustered, the trajectories inferred from multi-dimensional principle

226 components analysis, and the lineage projected onto the two-dimensional UMAP plot. (C-

227 D) Log_2 expression levels of *atilla* and *PPO3*. Relative expression levels were estimated

228 from normalized and scaled unique molecular identifier counts.

229

230

231 **Morphological differentiation of immune cells remains an inducible**
232 **response**

233 Lamellocytes are classically defined morphologically as large flattened cells. As
234 expected, the proportion of morphologically identifiable lamellocytes increased
235 after infection (Figs 5A and Fig. S11A; Treatment: χ^2= 48.14, d.f= 1, p=3.97x10^{-}
236 ^{12}). However, in contrast to our analysis of single cell transcriptomes, there was
237 little difference between selection regimes in either the induced or constitutive
238 proportion of these cells (Figs 5A and Fig. S11A; Selection regime x Treatment:
239 χ^2= 0.16, d.f= 1, p=0.69; Selection regime: χ^2= 0.41, d.f= 1, p=0.52). This suggests
240 that while the transcriptional state of cells has been constitutively activated, the
241 change in cell morphology remains an inducible response. To test this
242 hypothesis, we used microscopy to measure both cell morphology and, as a
243 marker of the transcriptional state of the cells, *atilla* expression (Fig. S12). In line
244 with our scRNAseq data, both infection and adaptation to high parasitism rates
245 increases the proportion of *atilla* positive cells (Fig. 5C; Selection Regime x
246 Treatment: F=16.3, d.f=1,8, p=0.004). However, among the *atilla* positive cells,
247 infection had a large effect on cell size (Fig. 5C; Treatment: F=31.8, d.f.=1,7,
248 p=0.0008), while selection had a small effect (Fig. 5C; Selection Regime: F=7.2,
249 d.f.=1,7, p=0.03). Therefore, while selection has resulted in the constitutive
250 transcriptional activation of cells, changes in cell morphology remain largely an
251 inducible response.

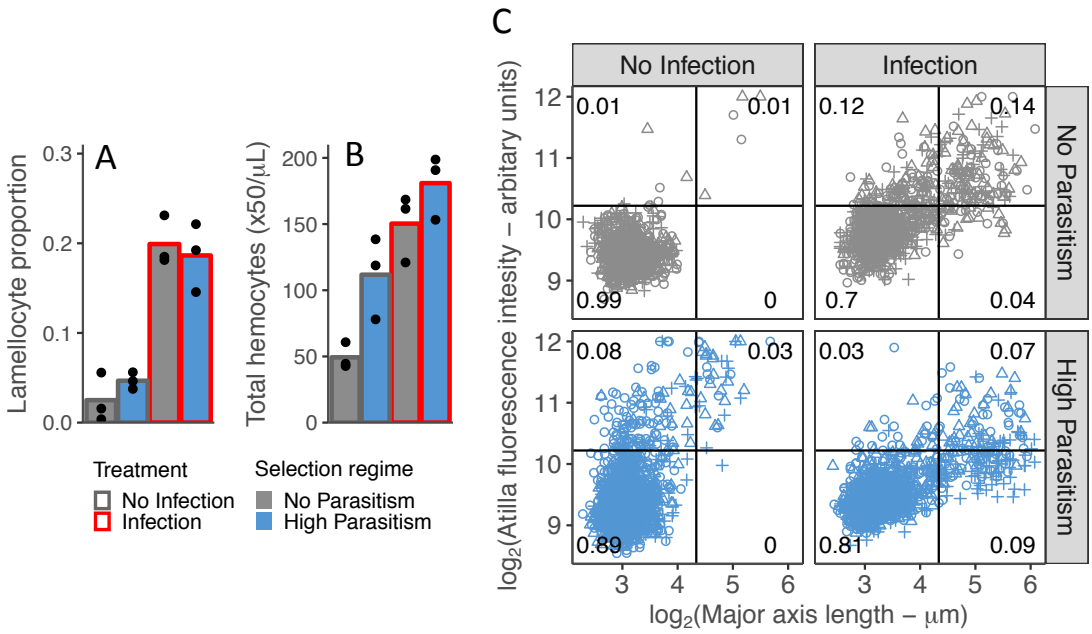

Figure 5. Changes in the morphology and number of cells following infection and adaptation to high parasitism rates. (A) The proportion hemocytes that were morphologically identified as lamellocytes and (B) the concentration of total circulating hemocytes in no infection conditions (grey outline) and 48 hours post infection (red outlines). Samples were collected from populations that evolved 34 generation with high parasitism (blue bars) or no parasitism (grey bars) (C) Cell size and *atilla* expression. The expression of *atilla* was measured as the fluorescence intensity resulting from immunohistochemistry staining. Cell size was measured along the major axis. Replicated populations from each selection regime are represented by different symbols and the proportion of cells in each quarter of the plot is shown.

In addition to the change in the transcriptional state of cells, we found that the populations maintained under strong parasite pressure evolved a constitutive increase in the absolute number of hemocytes in circulation (Fig. 5B and Fig. S11B, Selection regime: χ^2= 22.37, d.f= 1, p=2.25x10^{-6}). This supports results from previous selection experiments [13,27] and comparative analyses [28], and is another aspect of the induced response that has become constitutive.

Conclusions

Our results provide support for the hypothesis that natural selection favours constitutive defences when infection is common [5–7] by demonstrating that an inducible immune response becomes constitutive when populations frequently encounter a parasite. The induced immune response to parasitoids relies on the differentiation of lamellocytes from embryonic-derived plasmatocytes, lymph gland prohemocytes [8] and lymph gland plasmatocytes [18]. Evidence for immature lamellocytes has previously come from patterns of marker gene expression [29,30] and recent scRNAseq data [17,19]. Our results show that *Drosophila* populations evolve to produce these cells constitutively if they are frequently exposed to infection. However, this change in the transcriptional state of cells was not accompanied by morphological differentiation. Genes involved in cytoskeleton dynamics such as *βTub60D* and *shot* are among the genes with the greatest increases in expression as lamellocytes differentiate (Fig. S10, Data S4) and these may be required for the final step of changing cell shape [31]. Together, our results suggest populations that adapt to high parasitism rates have their cellular immune defences in a state of readiness, with the final step of cell differentiation remaining an inducible response.

Evolving resistance to parasitoid wasps is costly in *Drosophila* [12,14,32], so inducible immunity may be an adaptation that allows uninfected individuals to avoid this cost under low parasitism conditions. The physiological mechanism that causes the cost is unknown. It is possible that the differentiation of immature lamellocytes diverts resources from other fitness related traits. Lamellocyte differentiation is energy-demanding and results in the increased

295 expression of glycolysis genes in hemocytes after infection [3]. This cost may be
296 borne by uninfected flies in our resistant populations, as we found that genes
297 involved in trehalose uptake and catabolism [33], *Trehalase* and *Tret1-1*, are
298 upregulated by both infection and selection (Fig. S13). Another possibility is that
299 a more reactive cellular immune response may increase the effects of
300 immunopathology.
301
302 After infection, whether the host or parasitoid survives is a race between the
303 parasitoid development and the formation of a cellular capsule by the immune
304 system [34]. Constitutive differentiation of immature lamellocytes may allow
305 lamellocytes to be produced more rapidly upon infection. Furthermore, cytotoxic
306 molecules could be more readily available. This is supported by an increase in
307 the constitutive expression of *PPO3* in populations adapted to high rates of
308 parasitism. *PPO3* encodes a intracellular prophenoloxidase that, when active, is
309 responsible for the melanization of lamellocytes [9]. Along with the increase in the
310 total number of hemocytes, the constitutive activation of the cellular immune
311 response likely explains the greatly increased resistance of populations adapted
312 to high rates of parasitism.

313 **Methods**

314

315 **Artificial selection**

316 An outcrossed *D. melanogaster* population was founded from the progeny of 377
317 females collected in July 2018 from banana and yeast traps set up in an allotment
318 plot in Cambridge, UK (52°12'12.5"N 0°09'00.6"E). Single females were sorted
319 into vials with cornmeal food (per 1200ml water: 13g agar, 105g dextrose, 105g

320 maize, 23g yeast, 35ml Nipagin 10% w/v) to create isofemale lines. From the
321 progeny of each isofemale line, 5 females and 5 males lines were sorted into a
322 population cage to create the source population with 3770 flies. Flies from the
323 source population were allowed to lay eggs overnight in 90mm agar plates (per
324 1500ml water: 45g agar, 50g dextrose, 500ml apple juice, 30ml Nipagin 10%
325 w/v) spread with yeast paste (*Saccharomyces cerevisiae* – Sigma-Aldrich #YSC2).
326 Eggs were removed from the agar plate with phosphate buffered saline (PBS)
327 and a paintbrush, collected in 15ml centrifuge tubes and allowed to settle on the
328 bottom of the tube. 500µl of egg solution were transferred into a 1.5ml
329 microcentrifuge tube. 5µl of egg solution were transferred into plastic vials with
330 cornmeal food and incubated at 25°C, in a 14 hours light/10 hours dark cycle
331 and 70% humidity. 48 hours after egg transfer, a single female wasp was added
332 into vials for infection treatments and allowed to infect larvae for 24 hours. Vials
333 from infection and no infection treatments were incubated for 12 days in total.
334 Flies from infection treatment with visible capsules were collected and randomly
335 sorted into triplicate selection lines (NSRef1-3). Flies from no infection
336 treatment were sorted into triplicate control populations (C1-3). Consecutive
337 generations of selection were maintained with the same protocol described.
338 Population sizes were maintained at 200 adult flies for all populations, at
339 roughly 50% sex ratio.

340

341 **Estimation of encapsulation ratio**

342 To determine encapsulation ability, 10 vials per line were prepared without
343 infection and 20 vials with infection according to the selection protocol

344 described above. Flies emerging from the no infection vials (control flies) were
345 counted. Flies from infected vials were discriminated for the presence/absence
346 of capsules by squishing anesthetized flies between two glass slides and
347 observing under a dissecting microscope. Encapsulation ratio was calculated
348 according to the formula:

349 $$Encapsulation\ Ratio = \frac{Capsules}{Control - Uninfected}$$

350 In the formula, Capsules represent the mean number of flies from infection vials
351 with visible capsules and Uninfected represent the mean number of flies with no
352 discernable capsule. Control represent the mean number of flies from vials with
353 no infection. With this method we have an estimate of proportion of infected flies
354 with successful encapsulation per line.

355

356 **Wasp maintenance**

357 *Leptopilina boulardi* strain NSRef [35] was maintained in a very susceptible *D.*
358 *melanogaster* outbreed population named CAMOP2. Cornmeal vials were
359 prepared with 6µl of eggs as described above. Two female wasps and one male
360 were added to each vial. Vials were incubated for 24 days at 25°C, in a 14 hours
361 light/10 hours dark cycle and 70% humidity. Adult wasps were collected and
362 maintained in cornmeal vials with a drop of honey.

363

364 **Oil injection**

365 Egg solutions were prepared in 1.5ml microcentrifuge tubes as described above.
366 15µl of eggs were transferred into 50mm diameter plastic plates with cornmeal

367 food. Plates were incubated for 72h at 25°C. Borosilicate glass 3.5" capillaries
368 (Drummond Scientific Co. 3-000-203-G/X) were pulled to form thin needles in a
369 needle puller (Narishige PC-10). The needle was backfilled with paraffin oil
370 (Sigma-Aldrich #M5904) with a syringe and attached to a nanoinjector
371 (Drummond Scientific Co. Nonoject II). Late 2nd instar and early 3rd instar larvae
372 were carefully removed with forceps from cornmeal food plates and placed on
373 filter paper, in groups of 20. Larvae were carefully injected with 4.6nl of oil. After
374 injection, $_{dd}H_20$ was added with a brush to remove the larvae and a total of 40
375 larvae were transferred into a cornmeal food vial and incubated at 25°C. After 48
376 hours larvae were removed with a 15% w/v sugar solution and transferred into
377 $_{dd}H_2O$ droplets on top of a plastic plate. Larvae were observed under a dissecting
378 microscope and scored for the presence of melanization in the oil droplet.

379

380 **Hemocyte counts**

381 To estimate hemocyte concentration, eggs were transferred into cornmeal vials
382 following the artificial selection protocol described above and incubated at 25°C.
383 In infection treatment vials, 3 female wasps were allowed to infect larvae for 3
384 hours, 48 hours post egg transfer. This protocol guarantees a high infection ratio
385 [36] and reduces the time window for the treatment. Vials from all treatments were
386 incubated for a total of 4 days. 3rd instar larvae were collected from the food
387 vials, washed in $_{dd}H_2O$, dried in filter paper and transferred to a multispot
388 porcelain plate in groups of 10. Hemolymph was collected by tearing the larval
389 cuticle from the ventral side. 2µl of hemolymph were rapidly collected and
390 diluted in 8µl of Neutral Red (1.65g/L PBS – Sigma-Aldrich #N2889) to help

391 visualize the cells. The diluted hemolymph was transferred into a Thoma
392 chamber and the number of hemocytes in 0.1µl was counted. Plasmatocytes and
393 lamellocytes were distinguished by morphology [37].

394

395 **Quantitative PCR**

396 To analyze the expression of *PPO3* and *atilla*, RNA was extracted from hemocytes
397 pooled from 50-70 larvae, 24h post infection. Larvae were cleaned in $_{dd}H_2O$,
398 dried in filter paper and transferred into a well of a multispot porcelain plate
399 with 100µl of PBS. Hemolymph was collected by tearing the ventral side of the
400 larval cuticle. Samples were homogenized in 400µl TRIzol [Ambion #15596018]
401 and kept at -80°C. For RNA extraction, samples were defrosted and centrifuged
402 for 10min at 4°C at 12.000g. 160µl of supernatant was transferred into 1.5ml
403 microcentrifuge tubes, 62.5µl of chloroform [Fisher Scientific #C/4920/08] was
404 added, tubes were shaken for 15s and incubated for 3min. After a 10min
405 centrifugation at 12,000g at 4°C, 66µl of the aqueous phase was transferred into
406 a 1.5µl microcentrifuge tube, 156µl of isopropanol [Honeywell #33539] added
407 and the solution thoroughly mixed. After 10min incubation samples were
408 centrifuged for 10min at 12.000g at 4°C and the supernatant was removed. RNA
409 was washed with 250µl 70% ethanol, centrifuged for 2min at 12.000g at 4°C.
410 Ethanol was removed, samples dried, 20µl of nuclease free water [Ambion
411 #AM9930] was added and samples incubated at 45°C for 10min. cDNA was
412 prepared from RNA samples with GoScript reverse transcriptase (Promega)
413 according to manufacture instructions. cDNA was diluted 1:10. Exonic primers
414 for *D. melanogaster PPO3* and *atilla* were designed in NCBI Primer-BLAST online

415 tool: (PPO3_qPCR_2_Fw: 5'-GATGTGGACCGGCCTAACAA-3'; PPO3_qPCR_2_Rev 5'-
416 GATGCCCTTAGCGTCATCCA-3'; atilla_qPCR2_Fw: 5'-
417 ACCCACCAAATATGCTGAAACA-3'; atilla_qPCR2_Rv: TTGATGGCCGATGCACTGT).
418 The gene *RpL32* was used to normalize gene expression (RpL32_qPCR_F-d: 5'-
419 TGCTAAGCTGTCGCACAAATGG-3'; RpL_qPCR_R-h 5'-
420 TGCGCTTGTTCGATCCGTAAC-3'; [38]. Sensifast Hi-Rox SyBr kit (Bioline) was used
421 to perform the RT-qPCR on a StepOnePlus system (ThermoFisher Scientific).
422 Each sample was duplicated (qPCR technical replica). The PCR cycle was 95°C for
423 2min followed by 40 cycles of 95°C for 5s, 60°C for 30s.

424

425 **Hemocyte immunohistochemistry**

426 Larvae were prepared in the same conditions as for hemocyte counts, described
427 above. Larvae were washed in $_{dd}H_2O$, dried on filter paper and transferred into a
428 well of multispot porcelain plate with 25µl PBS. Hemolymph was collected by
429 tearing the ventral cuticle with forceps and the hemocyte suspension was
430 transferred into a reaction well of a microscope slide (Marienfeld, #1216330).
431 Samples were incubated for 30min in a humid chamber, fixed for 20 min with
432 3.8% formaldehyde (Sigma-Aldrich #F8775) and washed 3 times with PBS. Cells
433 were blocked and permeabilized with 0.01% Triton-X and 1% NGS diluted in
434 PBS for 30 min and washed 3 times with PBS. Primary antibody against *atilla*
435 (L1, 1:100, [39]) was added with 1% NGS overnight at 4°C. Primary antibody was
436 washed with PBS for 5 min 3 times and secondary antibody (Alexa Fluor 488,
437 anti-mouse, 1:1000) was applied overnight at 4°C. Cells were washed 3 times
438 with PBS and stained with Hoechst 33342 (Invitrogen #H3570, 1µg/ml) and

439 phalloidin (Alexa Fluor 594, Invitrogen #A12381, dilution 1:2000) for 30min.
440 After cells were washed 3 times with PBS, cover slides were mounted with
441 Vectashield (Vector laboratories).

442

443 **Image acquisition and analysis**

444 Images were acquired in a Leica DM6000 fluorescence microscope with a 40x
445 objective. Images were analyzed with Fiji version 1.0 [40]. Cells were identified
446 based on actin and nuclear staining and manually outlined with the selection
447 tool. Maximum intensity of *atilla* staining and length of the major axis was
448 recorded for each cell. The threshold for staining intensity was obtained by
449 measuring intensity of cells that were stained following the
450 immunohistochemistry protocol (described above) but with no primary
451 antibody. The threshold for cell size was obtained from a independent set of
452 images where cells were measured and classified as lamellocytes.

453

454 **Statistical analysis**

455 All statistical analyses were performed using R. Encapsulation proportions
456 during artificial selection were arcsine transformed and analyzed with a general
457 linear mixed effects model where selection treatment, generation and the
458 interaction term were considered fixed factors and population a random
459 variable. Oil melanization proportions were arcsine transformed and selection
460 regime was used as an explanatory variable in a linear model. To analyze *atilla*
461 and *PPO3* expression from qPCR results we used a mixed effects model with
462 treatment, selection regime and the interaction term as fixed effects and

463 population and target gene as random variables. Total hemocyte counts and the
464 arcsine transformed lamellocyte proportions were analyzed with mixed effects
465 models with treatment and selection regime as explanatory variables and
466 population as a random variable. Proportions of cells considered atilla^{+} with
467 immunohistochemistry staining were analyzed with a linear model with
468 treatment, selection regime and the interaction term as explanatory variables. In
469 all cases, significance was assessed with ANOVA.

470

471 **Hemocyte preparation for scRNAseq**

472 Larvae from both selection regimes and infection treatments were obtained
473 following the protocol for hemocyte counting, as described above. 80 to 140
474 larvae per biological replica were cleaned in PBS and dried on filter paper.
475 Larvae were transferred into 200µl PBS and dissected by tearing the ventral
476 cuticle. 200µl of hemocyte solution were collected and filtered (Flowmi cell
477 strainer 70µm). The cell suspension was carefully transferred into a 15ml
478 centrifuge tube with OptiPrep solution (Sigma-Aldrich D1556; 540µl OptiPrep
479 and 1460µl PBS). Samples were centrifuged at 170g for 20 min in a swinging
480 bucket centrifuge at 4°C with no brake. The first two layers of 100µl were then
481 carefully removed and hemocytes were counted in a Thoma chamber. The
482 sample fraction with more hemocytes was used for encapsulation in 10X single
483 cell platform at Cancer Research UK Cambridge Institute. Library preparation
484 was performed with standard protocols of single cell 3' V2 chemistry 10X
485 Genomics.

486

487 **Read alignments and cell detection**

488 Demultiplexed FASTQ data files were aligned to a custom-built *D. melanogaster*
489 reference obtained from FlyBase FB2018_02 Dmel Release 6.21 [41] and created
490 using the Cell Ranger pipeline (https://support.10xgenomics.com/single-cell-
491 gene-expression/software/overview/welcome, last accessed 23-03-2020). Less
492 than 1,000 cells were detected in libraries generated from control and selected
493 populations in one of the three replicates (replicate two). This replicate was
494 dropped in further analysis. 25,128 cells were identified across the two
495 remaining replicates. The entire sequence of data filtering and clustering is listed
496 in Fig. S14. Most of the analyses were done in R versions 3.6 [42] and we used the
497 Tidyverse, gridExtra and cowplot packages to manipulate and plot the data.

498

499 **Normalization, integration and dimensionality reduction**

500 Seurat version 3.1.1 [43] was used to process and analyze the single cell count
501 matrix. Unique molecular identifier (UMI) count matrices obtained from Cell
502 Ranger were normalized using a scaling factor of 10,000 and log-normal
503 transformation. 2,000 highly variable genes were discovered using the 'vst'
504 method (Data S6). Count matrices from individual samples were integrated
505 allowing for a maximum of 50 dimensions and 2,000 anchor features.

506 We identified 281 cells that expressed fewer than 250 features or more
507 than 2,500 features and 5,387 cells that did not express either *He* or *Srp*, two
508 pan-hemocyte markers [21]. These cells were removed from the constituent
509 samples. Following this, the count matrices were normalized, highly variable
510 features were identified, and the samples were re-integrated.

511

512 **Mean fold change in gene expression**

513 To combine data across cells to examine gene expression differences between
514 treatments, we performed the data integration steps utilizing all possible
515 anchors features in Seurat. In doing so, a total of 7,716 genes were used for
516 integrating the sample count matrices (Data S6). Fold changes in expression
517 between treatments were obtained from the output of *FindMarkers* with min.pct
518 and logfc.threshold both set to 0. The fold change was converted to a $\log_2$ scale
519 and plotted using the R package LSD.

520

521 **Clustering cells from scRNA-seq**

522 Cells were clustered in Seurat. First, expression levels were scaled and percent
523 mitochondria, number of features and UMI count per cell were regressed out.
524 Then, we performed PCA and UMAP dimensionality reductions allowing for 50
525 dimensions. We did a first round of clustering using the 'pca' reduction and a
526 clustering 'resolution' of 0.2. We identified markers upregulated in each cluster
527 using the function *FindAllMarkers* with 'min.pct' and 'logfc.threshold' both set to
528 0.25 and tested for differential expression using MAST [44]. We conduced
529 enrichment analyses on upregulated cluster markers using the Flymine database
530 and tool [45] with the 2,000 highly variable genes as the background list. We
531 identified significantly enriched gene ontology categories [46] and pathways from
532 the KEGG and Reactome [47,48] in each cluster.

533 Enrichment analyses from the first round of clustering indicated one
534 cluster, comprising of 28 cells, was highly enriched for sperm-cell expressed

535 genes (Data S7 - cluster 9). These cells were removed from the constituent
536 sample count matrices and the data were re-integrated. In the second round of
537 clustering, a 'resolution' of 0.3 was used and we discovered that cluster 9 (48
538 cells) and cluster 10 (41 cells) were enriched for genes associated with muscle
539 and fat body tissues, respectively (Data S8). These cells were removed from the
540 constituent sample count matrices and data were re-integrated. For round three
541 of clustering, a 'resolution' of 0.3 was utilized. At this point, the 19,344 remaining
542 cells were partitioned into nine clusters.

543 We identified the *D. melanogaster* orthologs of human cell cycle markers
544 identified in Tirosh et al. [49] using the EBI database [50]. The expression levels of
545 these cell cycle genes were used to classify cells by phase using the function
546 *CellCycleScoring* in Seurat. Regressing out the difference between the G2M and S
547 phases had a minimal impact on the cell cluster classification for all but one
548 cluster (Table S2). The greater discordance among the lamellocyte cluster CC-5 is
549 due to the placement of cells differentiating along a single lineage into discrete
550 clusters.

551 We tested if using all possible anchors rather than just the highly variable
552 ones had an impact on data integration and clustering. Clustering the data set the
553 7,716 anchors using the same resolution (0.3) largely revealed the same cell
554 clusters save for the appearance of two very small clusters comprising of 113
555 and 56 cells (cluster 9 and 10 - Table S3). Also, this data set showed that the
556 proportion of lamellocytes (represented by clusters 1,2,4 and 5) increased
557 following high parasitism and infection (Fig. S15) suggesting the choice of
558 anchors did not result in erroneous patterns. When necessary, we converted the

559 Flybase IDs to gene symbols using the org.Dm.eg.db database v.3.7 [51]. The R
560 package reshape2 [52] was used to estimate proportions of cells in each cluster.
561
562 **Subclustering lamellocytes**
563 We performed subclustering on lamellocytes and their plasmatocyte progenitors
564 to better resolve the trajectory of cell differentiation. Clusters 1, 2, 4 and 5 from
565 round three clustering had enriched expression of described lamellocyte
566 markers (*ItgaPS4*, *atilla*, *mys*, *PPO3* - [21]) and, therefore, these cells were isolated
567 for subclustering (Fig. S16). Cluster 0 from round three clustering was identified
568 as the progenitor plasmatocyte population based on the expression of five
569 plasmatocyte markers (*Col4a1*, *Pxn*, *eater*, *Hml*, *NimC1* - [21]) and three cell cycle
570 markers (*stg* – [22], *polo* – [23]and *scra* – [24]) (Fig. S17).
571 The presumed lamellocytes and plasmatocyte progenitor were subset
572 from the constituent sample count matrices. The cell count matrices for each
573 sample were normalized and 2,000 highly variable features were found.
574 Following this, dimensionality reduction and round one of subclustering was
575 performed using a 'resolution' parameter of 0.3. In round one of subclustering,
576 we identified 79 cells that were significantly enriched for markers representing
577 crystal cells (Fig. S18 & Data S9 - cluster 5). These cells were moved to the
578 crystal cell cluster and we did a second round of subclustering on the remaining
579 cells. We followed the same data integration and clustering steps but used a
580 resolution of 0.2. The original cluster identities for lamellocytes and
581 plasmatocyte progenitor cells were replaced with their new identities inferred
582 from the subclustering.

583

584 **Trajectory inference**

585 We used the software Slingshot [53] to conduct pseudotime analysis. We used all
586 50 PCA dimensions estimated from Seurat for trajectory inference and ensured
587 lineages were not inferred past endpoints by setting stretch to 0. The cluster
588 with the highest expression of the three cell cycle markers (*stg*, *polo* and *scra*)
589 was set as starting cluster.

590 2000 highly variable genes were utilized for identifying lineage markers.
591 A random forest model was fit to identify the genes best able to predict the
592 pseudotime values using R tidymodels. The R package 'Ranger' was used for
593 implementation of the random forest using mtry = 200, trees = 1400, and min_n
594 = 15 and variable importance was ranked by Gini impurity.

595

596 **Cluster definitions**

597 We performed pathway enrichment analyses on all non-lamellocyte clusters
598 with the aim of defining them according to their inferred biological function.
599 First, upregulated cluster markers were identified through pairwise differential
600 expression tests. The cluster of interest was compared with PLASM1 using the
601 function *FindMarkers* with 'min.pct' and 'logfc.threshold' both set to 0.25. Genes
602 with significant upregulation in each cluster were identified using the MAST test
603 statistic (Data S10) after performing Bonferroni correction on the obtained *P*-
604 values. Markers upregulated in each cluster were used for pathway enrichment
605 analysis. Markers for the plasmatocyte progenitor population were identified
606 through comparisons to the cell types containing other plasmatocyte-type cells.

607 These markers were used for pathway enrichment analyses using the approach
608 described in previous sections.
609
610
611 **References**
612

613 1. Savage, H. P. *et al.* Blimp-1-dependent and -independent natural antibody
614 production by B-1 and B-1-derived plasma cells. *J. Exp. Med.* **214**, 2777–
615 2794 (2017).

616 2. Lemaitre, B. & Hoffmann, J. The host defense of Drosophila melanogaster.
617 *Annu. Rev. Immunol.* **25**, 697–743 (2007).

618 3. Bajgar, A. *et al.* Extracellular Adenosine Mediates a Systemic Metabolic
619 Switch during Immune Response. *PLoS Biol.* **13**, 1–23 (2015).

620 4. Graham, A. L., Allen, J. E. & Read, A. F. Evolutionary causes and
621 consequences of immunopathology. *Annu. Rev. Ecol. Evol. Syst.* **36**, 373–
622 397 (2005).

623 5. Shudo, E. & Iwasa, Y. Inducible defense against pathogens and parasites:
624 Optimal choice among multiple options. *J. Theor. Biol.* **209**, 233–247
625 (2001).

626 6. Boots, M. & Best, A. The evolution of constitutive and induced defences to
627 infectious disease. *Proc. R. Soc. B Biol. Sci.* **285**, (2018).

628 7. Westra, E. R. *et al.* Parasite exposure drives selective evolution of
629 constitutive versus inducible defense. *Curr. Biol.* **25**, 1043–1049 (2015).

630 8. Honti, V., Csordás, G., Kurucz, É., Márkus, R. & Andó, I. The cell-mediated
631 immunity of Drosophila melanogaster: hemocyte lineages, immune
632 compartments, microanatomy and regulation. *Dev. Comp. Immunol.* **42**,
633 47–56 (2014).

634 9. Dudzic, J. P., Kondo, S., Ueda, R., Bergman, C. M. & Lemaitre, B. Drosophila
635 innate immunity: regional and functional specialization of
636 prophenoloxidases. *BMC Biol.* **13**, 81–97 (2015).

637 10. Nappi, A. J., Poirié, M. & Carton, Y. The Role of Melanization and Cytotoxic
638 By-Products in the Cellular Immune Responses of Drosophila Against
639 Parasitic Wasps. in *Advances in Parasitology* 99–121 (2009).

640 11. Kraaijeveld, A. R. & Godfray, H. C. J. Geographic Patterns in the Evolution of
641 Resistance and Virulence in Drosophila and Its Parasitoids. *Am. Nat.* **153**,
642 S61–S74 (1999).

643 12. McGonigle, J. E. *et al.* Parallel and costly changes to cellular immunity
644 underlie the evolution of parasitoid resistance in three Drosophila species.
645 *PLoS Pathog.* **13**, (2017).

646 13. Kraaijeveld, A. R., Limentani, E. C. & Godfray, H. C. Basis of the trade-off
647 between parasitoid resistance and larval competitive ability in Drosophila
648 melanogaster. *Proc. Biol. Sci.* **268**, 259–61 (2001).

649 14. Fellowes, M. D., Kraaijeveld, A. R. & Godfray, H. C. Trade-off associated with
650 selection for increased ability to resist parasitoid attack in Drosophila
651 melanogaster. *Proc Biol Sci* **265**, 1553–1558 (1998).

652 15. Havard, S., Eslin, P., Prévost, G. & Doury, G. Encapsulation ability: Are all

653 *Drosophila* species equally armed? An investigation in the *obscura* group.
654 *Can. J. Zool.* **87**, 635–641 (2009).

655 16. Fu, Y., Huang, X., Zhang, P., Leemput, J. Van De & Han, Z. Single-cell RNA
656 sequencing identifies novel cell types in Drosophila blood. *J. Genet.*
657 *Genomics* (2020) doi:10.1016/j.jgg.2020.02.004.

658 17. Gopal Tattikota, S. *et al.* A single-cell survey of Drosophila blood. *bioRxiv*
659 (2019) doi:10.1101/2019.12.20.884999.

660 18. Cho, B. Single-cell transcriptome maps of myeloid blood cell lineages in
661 Drosophila. *bioRxiv* (2020).

662 19. Cattenoz, P. B. *et al.* Temporal specificity and heterogeneity of Drosophila
663 immune cells . *EMBO J.* 1–25 (2020) doi:10.15252/embj.2020104486.

664 20. Vivancos, R. B. V. & Giangrande, A. glide/gcmIs Expressed and Required in
665 the Scavenger Cell Lineage. *Dev. Biol.* **191**, 118–130 (1997).

666 21. Banerjee, U., Girard, J. R., Goins, L. M. & Spratford, C. M. *Drosophila* as a
667 Genetic Model for Hematopoiesis. *Genetics* **211**, 367–417 (2019).

668 22. Edgar, B. A. & O'Farrell, P. H. The three postblastoderm cell cycles of
669 Drosophila embryogenesis are regulated in G2 by string. *Cell* **62**, 469–480
670 (1990).

671 23. Glover, D. M. Polo kinase and progression through M phase in Drosophila:
672 a perspective from the spindle poles. *Oncogene* **24**, 230–237 (2005).

673 24. Oegema, K., Savoian, M. S., Mitchison, T. J. & Field, C. M. Functional Analysis
674 of a Human Homologue of the Drosophila Actin Binding Protein Anillin
675 Suggests a Role in Cytokinesis. *J. Cell Biol.* **150**, 539–552 (2000).

676 25. Olofsson, B. & Page, D. T. Condensation of the central nervous system in
677 embryonic Drosophila is inhibited by blocking hemocyte migration or
678 neural activity. *Dev. Biol.* **279**, 233–243 (2005).

679 26. Bunt, S. *et al.* Hemocyte-Secreted Type IV Collagen Enhances BMP
680 Signaling to Guide Renal Tubule Morphogenesis in Drosophila. *Dev. Cell* **19**,
681 296–306 (2010).

682 27. Mcgonigle, J. E. *et al.* Parallel and costly changes to cellular immunity
683 underlie the evolution of parasitoid resistance in three Drosophila species.
684 *PLoS Pathog.* **13(10)**, 1–20 (2017).

685 28. Eslin, P. & Prevost, G. Hemocyte load and immune resistance to Asobara
686 tabida are correlated in species of the Drosophila melanogaster subgroup.
687 *J. Insect Physiol.* **44**, 807–816 (1998).

688 29. Honti, V. *et al.* Cell lineage tracing reveals the plasticity of the hemocyte
689 lineages and of the hematopoietic compartments in Drosophila
690 melanogaster. *Mol. Immunol.* **47**, 1997–2004 (2010).

691 30. Anderl, I. *et al.* Transdifferentiation and Proliferation in Two Distinct
692 Hemocyte Lineages in Drosophila melanogaster Larvae after Wasp
693 Infection. *PLoS Pathog.* **12**, 1–34 (2016).

694 31. Rizki, T. M. & Rizki, R. M. Parasitoid-induced cellular immune deficiency in
695 Drosophila. *Ann. N. Y. Acad. Sci.* **712**, 178–94 (1994).

696 32. Kraaijeveld, A. R. & Godfray, H. C. Trade-off between parasitoid resistance
697 and larval competitive ability in Drosophila melanogaster. *Nature* **389**,
698 278–280 (1997).

699 33. Mattila, J. & Hietakangas, V. Regulation of carbohydrate energy metabolism
700 in Drosophila melanogaster. *Genetics* (2017)
701 doi:10.1534/genetics.117.199885.

702 34. Kim-Jo, C., Gatti, J. L. & Poirié, M. Drosophila cellular immunity against
703 parasitoid wasps: A complex and time-dependent process. *Front. Physiol.*
704 **10**, (2019).

705 35. Varaldi, J., Petit, S., Boulétreau, M. & Fleury, F. The virus infecting the
706 parasitoid Leptopilina boulardi exerts a specific action on superparasitism
707 behaviour. *Parasitology* **132**, 747–756 (2006).

708 36. Leitão, A. B. *et al.* Independent effects on cellular and humoral immune
709 responses underlie genotype-by-genotype interactions between
710 Drosophila and parasitoids. *PLoS Pathog.* **15**, 1–13 (2019).

711 37. Rizki, T. M. Alterations in the haemocyte population of Drosophila
712 melanogaster. *J. Morphol.* **100**, 437–458 (1957).

713 38. Longdon, B. *et al.* The Causes and Consequences of Changes in Virulence
714 following Pathogen Host Shifts. *PLoS Pathog.* **11**, 1–18 (2015).

715 39. Kurucz, É. *et al.* Definition of Drosophila hemocyte subsets by cell-type
716 specific antigens. *Acta Biol. Hung.* **58**, 95–111 (2007).

717 40. Schindelin, J. *et al.* Fiji: An open-source platform for biological-image
718 analysis. *Nature Methods* vol. 9 676–682 (2012).

719 41. Thurmond, J. *et al.* FlyBase 2.0: the next generation. *Nucleic Acids Res.* **47**,
720 D759–D765 (2019).

721 42. R Core Team. A language and environment for statistical computing. R

722 Foundation for Statistical Computing, Vienna, Austria. *https://www.R-*
723 *project.org/* (2018).

724 43. Stuart, T. *et al.* Comprehensive Integration of Single-Cell Data. *Cell* **177**,
725 1888-1902.e21 (2019).

726 44. Finak, G. *et al.* MAST: a flexible statistical framework for assessing
727 transcriptional changes and characterizing heterogeneity in single-cell
728 RNA sequencing data. *Genome Biol.* **16**, 278 (2015).

729 45. Lyne, R. *et al.* FlyMine: an integrated database for Drosophila and
730 Anopheles genomics. *Genome Biol.* **8**, R129 (2007).

731 46. Huang, D. W., Sherman, B. T. & Lempicki, R. A. Bioinformatics enrichment
732 tools: paths toward the comprehensive functional analysis of large gene
733 lists. *Nucleic Acids Res.* **37**, 1–13 (2009).

734 47. Kanehisa, M. *et al.* From genomics to chemical genomics: new
735 developments in KEGG. *Nucleic Acids Res.* **34**, D354–D357 (2006).

736 48. Fabregat, A. *et al.* The Reactome pathway Knowledgebase. *Nucleic Acids*
737 *Res.* **44**, D481–D487 (2016).

738 49. Tirosh, I. *et al.* Dissecting the multicellular ecosystem of metastatic
739 melanoma by single-cell RNA-seq. *Science (80-.).* **352**, 189–196 (2016).

740 50. Madeira, F. *et al.* The EMBL-EBI search and sequence analysis tools APIs in
741 2019. *Nucleic Acids Res.* **47**, W636–W641 (2019).

742 51. Carlson, M. org.Dm.eg.db: Genome wide annotation for Fly. *R Packag.*
743 *version 3.7.0.* (2018).

744 52. Wickham, H. Reshaping Data with the **reshape** Package. *J. Stat. Softw.* **21**,

745 (2007).

746 53. Street, K. *et al.* Slingshot: cell lineage and pseudotime inference for single-
747 cell transcriptomics. *BMC Genomics* **19**, 477 (2018).

748

749 **Acknowledgements:** The Genomics Core Facility at Cancer Research UK
750 Cambridge Institute, G. Raddi and S. Tattikota provided protocols for the
751 scRNAseq. **Funding:** This work was funded by Natural Environment Research
752 Council grant NE/P00184X/1 to FJ and AL, an EMBO Postdoctoral Fellowship to
753 AL (ALT-1556) and a Natural Sciences and Engineering Research Council of
754 Canada Postdoctoral Fellowship (PDF-516634-2018, Committee: 187) to RA.
755 **Competing Interests:** None. **Author Contributions:** AL, RA and FMJ designed
756 the study and wrote the paper with input from the other authors. AL, JD and EG
757 performed the *Drosophila* work. AL and JD generated the sequencing data. RA
758 analysed the sequence data. **Data and materials availability:** Unprocessed
759 single cell sequence reads were deposited in the Sequence Read Archive
760 (accession: SRP256887, Bioproject: PRJNA625925). Cell count matrices for all
761 detected genes, cluster identities and processed scRNA-seq results were
762 deposited into Gene Expression Omnibus (accession: GSE148826). The R script
763 used to analyze the scRNA-seq data is available on Github (Repository:
764 dmel_scRNA_hemocyte).